

Extracting single electron wavefunctions from a quantum electrical current

A. Marguerite¹, B. Roussel², R. Bisognin¹, C. Cabart², M. Kumar¹, J.-M. Berroir¹, E. Bocquillon¹, B. Plaçais¹, A. Cavanna³, U. Gennser³, Y. Jin³, P. Degiovanni², and G. Fève^{1*}
¹Laboratoire Pierre Aigrain, Ecole Normale Supérieure-PSL Research University, CNRS, Université Pierre et Marie Curie-Sorbonne Universités, Université Paris Diderot-Sorbonne Paris Cité,
24 rue Lhomond, 75231 Paris Cedex 05, France.

² Univ Lyon, Ens de Lyon, Université Claude Bernard Lyon 1, CNRS,
Laboratoire de Physique, F-69342 Lyon, France.

³ Centre de Nanosciences et de Nanotechnologies, CNRS, Univ. Paris-Sud, Université Paris-Saclay,
C2N-Marcoussis, 91460 Marcoussis, France.

* To whom correspondence should be addressed; E-mail: feve@lpa.ens.fr.

Quantum nanoelectronics has entered an era where quantum electrical currents are built from single to few on-demand elementary excitations. To date however, very limited tools have been implemented to characterize them. In this work, we present a quantum current analyzer able to extract single particle excitations present within a periodic quantum electrical current without any a priori hypothesis. Our analyzer combines two-particle interferometry and signal processing to extract the relevant electron and hole wavefunctions localized around each emission period and their quantum coherence from one emission period to the other. This quantum current analyzer opens new possibilities for the characterization and control of quantum electrical currents in nanoscale conductors and for investigations of entanglement in quantum electronics down to the single electron level.

Can we extract the full single particle content of a quantum electrical current? Although growing in importance by the availability of on-demand single to few electron sources¹⁻⁴, characterizing the excitations of a quantum electrical current is still an open problem. In the stationary regime, electronic transport is described in term of coherent scattering of electronic modes characterized by their energies⁵. The knowledge of the mode population given by the electronic distribution function is then sufficient to predict any single-particle physical quantity. In the non-stationary regime, slow drives generate quasi-classical currents carrying a large number of excitations per period, which can also be viewed as adiabatic evolutions of the d.c. case. Conversely, fast drives lead to fully quantum electrical currents that can be used to transmit information carried by single to few electronic excitations transferred coherently during each period of the source. From a basic quantum physics perspective, as well as in terms of quantum technological applications, it is then natural to ask what their wavefunctions and what their injection probabilities are.

Beyond time^{1,6} and energy distribution measurements^{4,7}, which are not able to answer these questions completely, theoretical works have investigated the elementary events of charge transfer through a quantum point contact⁸. Recent experimental works have probed electron and hole wavefunctions in a tunnel junction under a.c. excitation⁹ or have reconstructed the electronic Wigner distribution¹⁰ of a Leviton excitation^{3,11,12}. However, in both cases, the characterization of the input state is based on strong assumptions and cannot extract the electron and hole wavefunctions from an arbitrary quantum electrical current.

In this article, we present an on-chip quantum electrical current analyzer combining two-particle interferometry¹³⁻¹⁶ with signal processing techniques to answer these questions. The single particle content of a quantum electrical current is en-

coded within the electronic Wigner distribution^{6,18} which is a very relevant tool for describing quantum states, in particular of light¹⁹, atoms²⁰ or molecules²¹. Using sinusoidal drives for demonstration, we reconstruct the Wigner distributions of both a quasi-classical and a quantum electrical current. In the latter case, we extract the single particle wavefunctions from the reconstructed Wigner distribution as well as their coherence across different periods. This experiment demonstrates our ability to extract the full single particle content of a quantum current from experimental data without any assumption on the electronic state, opening new perspectives for electron and microwave quantum optics in conjunction with quantum information in quantum conductors.

Similarly to the electronic distribution function $f(\omega)$, which describes the occupation probability of electronic modes as a function of energy $\hbar\omega$ and contains all the single-body properties of a stationary current, the Wigner distribution $W^{(e)}(t, \omega)$ encodes all the single-particle properties of the electronic state in the non-stationary case. It also provides a direct way to distinguish between quasi-classical and quantum currents⁶. Quasi-classical currents are characterized by bounded values of the Wigner distribution, $0 \leq W^{(e)}(t, \omega) \leq 1$, such that $W^{(e)}(t, \omega)$ can be interpreted as a time-dependent electronic distribution function. Conversely, deviations from these classical bounds are the hallmark of the quantum regime where $W^{(e)}(t, \omega)$ can be used to extract electron and hole wavefunctions. Following the protocol presented in Ref.²², an unknown Wigner distribution can be reconstructed using an electronic Hong-Ou-Mandel²³ interferometer^{15,16}, which measures the overlap between two electronic states propagating towards the two inputs of a beam-splitter. The interferometer is implemented in a two-dimensional electron gas in the quantum Hall regime at filling factor $\nu = 2$. A quantum point contact is used as an electronic beam-splitter partitioning the outer edge channel. As can be seen on the sketch of

the experiment represented in Figure 1, the source generating the unknown state labeled by the subscript S is propagating in input 1 whereas input 2 is fed with a set of reference states called probe states and labeled $\{P_n\}, n \in \mathbb{N}$. The low frequency current noise at the output of the splitter probes the degree of indistinguishability between the source and probe states. To isolate the contribution of the source, we measure the excess noise ΔS at splitter output 3 between the on and off states of the source:

$$\Delta S = 2e^2 \mathcal{T}(1 - \mathcal{T}) \int \frac{d\omega}{2\pi} \left[\overline{\Delta W_S^{(e)}(t, \omega)} (1 - 2f_{\text{eq}}) - 2\overline{\Delta W_S^{(e)} \Delta W_{P_n}^{(e)}} \right] \quad (1)$$

where \mathcal{T} is the beam-splitter transmission, $\overline{\dots}^t$ denotes the average over time t and $\Delta W_{S/P_n}^{(e)}$ are respectively the source and probe excess Wigner distribution with respect to the equilibrium situation described by the Fermi-Dirac distribution: $W_{S/P_n}^{(e)}(t, \omega) = f_{\text{eq}}(\omega) + \Delta W_{S/P_n}^{(e)}(t, \omega)$. The first term in Eq.(B1) represents the classical random partition noise of the source. It is reduced by the second term which represents two-particle interferences between source and probe related to the overlap between $\Delta W_S^{(e)}$ and $\Delta W_{P_n}^{(e)}$. By properly choosing the probe states, Eq.(B1) allows for the reconstruction of any unknown Wigner distribution^{6,22}.

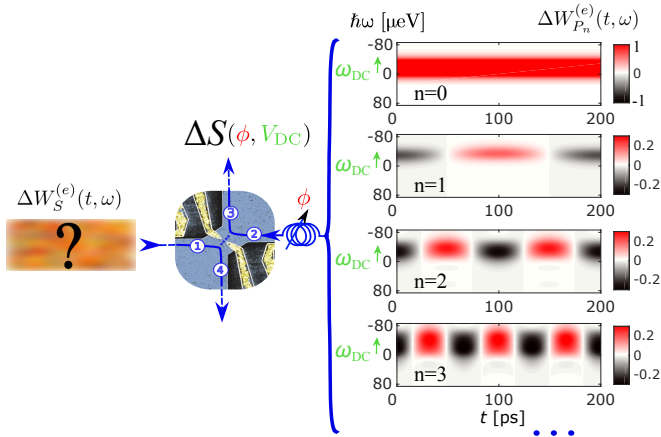


FIG. 1. The unknown Wigner distribution $\Delta W_S^{(e)}(t, \omega)$ is sent into input 1. The probe signals $\Delta W_{P_n}^{(e)}(\omega)$ sent into input 2 are plotted for $n = 0$ to $n = 3$, time (energy) is on the horizontal (vertical) axis. The frequency is $f = 5$ GHz and the temperature $T_{\text{el}} = 80$ mK). The excess noise ΔS is measured in output 3 as a function of the d.c. bias $V_{\text{DC}} = -\hbar\omega_{\text{DC}}/e$ and the phase difference ϕ between the source and probe signals.

As a proof of concept of our quantum current analyzer, we use simple sinusoidal drives, $V_S(t) = V_S \cos(2\pi ft)$ at various frequencies $f = 1/T$, a convenient choice which does not affect the generality of our results. In this case, the low frequency drives with $hf \lesssim k_B T_{\text{el}}$ (where $T_{\text{el}} = 100$ mK is the electronic temperature) are in the quasi-classical regime. $W_S^{(e)}$ should then be given by a Fermi sea with a time dependent chemical potential following the a.c. drive: $W_S^{(e)}(t, \omega) =$

$f_{\text{eq}}(\omega + \frac{eV_S}{\hbar} \cos(2\pi ft))$. Conversely, $hf \gtrsim k_B T_{\text{el}}$ corresponds to the quantum regime where deviations from the classical bounds are expected. As the source state is periodically emitted, a convenient choice of probe states basis is suggested by a Fourier expansion of the source Wigner distribution: $\Delta W_S^{(e)}(t, \omega) = \sum_n \Delta W_{S,n}^{(e)}(\omega) e^{2\pi i n f t}$. Let us first focus on the $n = 0$ harmonic, $\Delta W_{S,0}^{(e)}(\omega)$, which represents the source excess electronic distribution function. This time averaged quantity can be extracted from Eq.(B1) by using a d.c. bias V_{DC} as the probe P_0 (see Fig.1) so that $\Delta W_{P_0}^{(e)}(t, \omega) = f_{\text{eq}}(\omega - \omega_{\text{DC}}) - f_{\text{eq}}(\omega)$ (with $\omega_{\text{DC}} = -eV_{\text{DC}}/\hbar$) is very close to 1 for $0 \leq \omega \leq \omega_{\text{DC}}$ and to 0 elsewhere. Fig.2 (upper left panel) represents the excess noise ΔS as a function of ω_{DC} for various sinusoidal source drives of increasing frequency (1.75 GHz, 9 GHz and 20 GHz) with drive amplitudes ($V_S = 28 \mu\text{V}$, $31 \mu\text{V}$ and $38 \mu\text{V}$ respectively) chosen to produce similar partition noise (around $2 \times 10^{-29} \text{ A}^2 \text{ Hz}^{-1}$) at $\omega_{\text{DC}} = 0$ (P_0 switched off). The partition noise is suppressed to zero by two-electron interferences when the d.c. bias is increased but in different ways for different frequencies. $\Delta W_{S,0}^{(e)}(\omega)$ can then be obtained via the derivative of ΔS with respect to ω_{DC} ^{22,24} (see Supplementary Material). The obtained values of $\Delta W_{S,0}^{(e)}(\omega)$ are plotted on the upper right panel of Figure 2. The three curves show that as the drive frequency increases, the spectral weight is shifted towards higher frequencies. In the quasi-classical case ($f = 1.75$ GHz), the typical energy at which electrons (respectively holes) are promoted above (respectively below) the Fermi energy is given by the amplitude $eV_S = 28 \mu\text{eV}$ of the chemical potential variations. On the contrary, in the quantum regime ($f = 20$ GHz so that $hf > k_B T_{\text{el}}$), electron/hole pair creation results from the absorption of photons at energy hf ^{26,27}. The excess electron distribution function presents square steps of width $hf = 83 \mu\text{eV}$ and amplitude $(eV_S/hf)^2/4$, which is the probability to absorb one photon from the drive. Our experimental results compare very well with photo-assisted noise calculations²⁷ (plain lines) without any adjustable parameters, thus confirming the robustness of our measurement of $\Delta W_{S,0}^{(e)}(\omega)$.

Accessing the time dependence of $W_S^{(e)}(t, \omega)$ requires measuring the non-zero harmonics $\Delta W_{S,n \neq 0}^{(e)}$. Fortunately, an accurate reconstruction is usually achieved already with $|n| \leq 3$. Following Eq.(B1), accessing the n th harmonic requires a probe P_n whose Wigner distribution $W_{P_n}^{(e)}$ evolves periodically in time at frequency nf . At low excitation amplitude, the $W_{P_n}^{(e)}$ depends linearly on the probe voltage, $V_{P_n}(t) = V_{P_n} \cos(2\pi n f t + \phi)$, chosen to extract $\Delta W_{S,n}^{(e)}$:

$$\Delta W_{P_n}^{(e)}(t, \omega) = -\frac{eV_{P_n}}{\hbar} \cos(2\pi n f t + \phi) g_n(\omega - \omega_{\text{DC}}), \quad (2)$$

with $g_n(\omega) = (f_{\text{eq}}(\omega - n\pi f) - f_{\text{eq}}(\omega + n\pi f))/(2\pi n f)$. $\Delta W_{P_n}^{(e)}$ for $n = 1$ to $n = 3$ are plotted on Fig. 1. Changing the phase ϕ allows us to scan the temporal axis, whereas the width of $\Delta W_{P_n}^{(e)}$ along the energy axis is fixed by the width

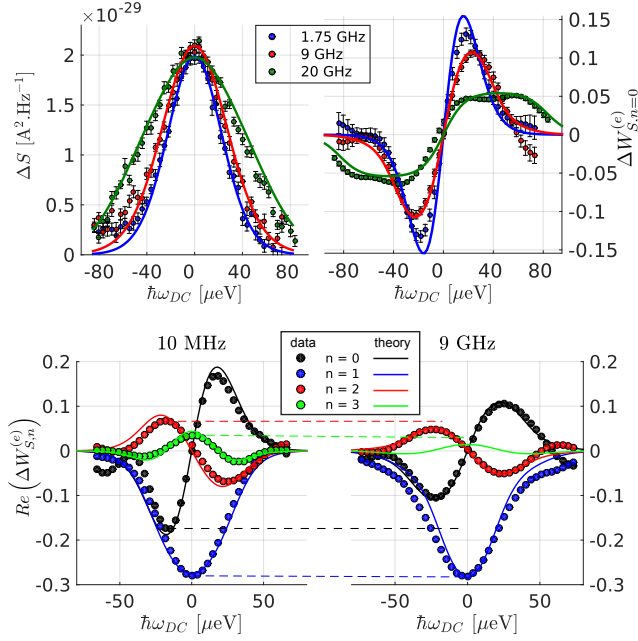


FIG. 2. Upper left panel: Excess noise ΔS as a function of d.c. bias ω_{DC} . The plain lines represent numerical calculations for $V_S = 28 \mu\text{V}$, $f = 1.75 \text{ GHz}$, $V_S = 31 \mu\text{V}$, $f = 9 \text{ GHz}$, and $V_S = 38 \mu\text{V}$, $f = 20 \text{ GHz}$ and $T_{el} = 100 \text{ mK}$. Upper right panel: electronic distribution function $\Delta W_{S,0}^{(e)}(\omega)$. Plain lines represent numerical calculations (same parameter as the left panel). Lower panel: $\Delta W_{S,n}^{(e)}(\omega)$ for $f = 10 \text{ MHz}$ (left) and $f = 9 \text{ GHz}$ (right). The plain lines represent numerical calculations with $T_{el} = 100 \text{ mK}$, $V_S = 33 \mu\text{V}$ ($f = 10 \text{ MHz}$) and $V_S = 31 \mu\text{V}$ ($f = 9 \text{ GHz}$).

of g_n , given by the maximum of $k_B T_{el}$ and nhf . As in the $n = 0$ case, varying a d.c. bias V_{DC} on top of the a.c. probe excitation enables scanning the energy axis. Using Eqs. (B1) and (2), the real and imaginary parts of $\Delta W_{S,n}^{(e)}$ can be directly related to the variations of ΔS as a function of the phase ϕ and d.c. bias V_{DC} (see Supplementary Material).

Figure 2 presents $\Re(\Delta W_{S,n}^{(e)})$ ($\Im(\Delta W_{S,n}^{(e)}) = 0$) for $n = 0, 1, 2, 3$ for a quasi-classical drive $f = 10 \text{ MHz}$ (lower left panel), and $n = 0, 1, 2$ ($n = 3$ falls below our experimental resolution) for a quantum drive $f = 9 \text{ GHz}$ (lower right panel). While the $n = 1$ harmonics take very close values as explained by the similar amplitudes of the drives ($V_S = 33 \mu\text{V}$ for $f = 10 \text{ MHz}$ and $V_S = 31 \mu\text{V}$ for $f = 9 \text{ GHz}$), the $n = 0, 2$ and 3 harmonics are lower in the high frequency case compared to the low frequency one. Indeed, these terms are related to multiphoton absorption/emission processes, whose strength increases with the ratio $\alpha = eV_S/hf$. This ratio is very high in the quasi-classical case ($\alpha \approx 800$) and smaller than one in the quantum one ($\alpha \approx 0.8$) thus explaining the smaller amplitude of the harmonics $n \neq 1$. After extracting all relevant $\Delta W_{S,n}^{(e)}$, we can combine them to reconstruct the full Wigner

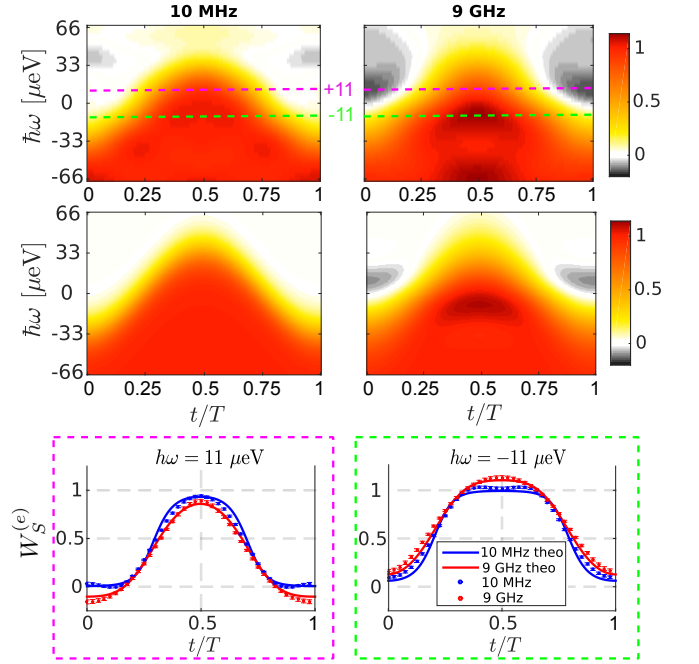


FIG. 3. Upper panels: experimental data of $W_S^{(e)}(t, \omega)$ in the quasi-classical ($f = 10 \text{ MHz}$, left) and quantum ($f = 9 \text{ GHz}$, right) cases. Middle panels: theoretical calculations of $W_S^{(e)}(t, \omega)$ at $f = 10 \text{ MHz}$ (left) and $f = 9 \text{ GHz}$ (right). Lower panels: cuts of $W_S^{(e)}(t, \omega)$ at constant energy $\hbar\omega = 11 \mu\text{eV}$ (left) and $\hbar\omega = -11 \mu\text{eV}$ (right). Blue points are for $f = 10 \text{ MHz}$, red points for $f = 9 \text{ GHz}$, the plain lines represent numerical calculations.

distribution:

$$W_S^{(e)}(t, \omega) = f_{eq}(\omega) + \Delta W_{S,0}^{(e)}(\omega) + 2 \sum_{n=1}^N \Re(\Delta W_{S,n}^{(e)}(\omega)) \cos(2\pi nft), \quad (3)$$

where the sum extends to $N = 3$ at $f = 10 \text{ MHz}$ and $N = 2$ at $f = 9 \text{ GHz}$, and where $\Im(\Delta W_{S,n}^{(e)}) = 0$ has been used. The two Wigner distributions are represented on Fig. 3 (upper panel). Apart for small discrepancies related to the deconvolution process, the quasi-classical case is very close to the expected equilibrium distribution function with a time varying chemical potential $\mu(t) = -eV_S \cos(2\pi ft)$ (see middle left panel). In particular, it is basically constrained to values between 0 and 1. In contrast, in the quantum case, the Wigner distribution can take values that are strongly negative or that are well above one. Consequently, single-particle properties are no longer described in terms of a time varying electronic distribution function, in good agreement with theoretical predictions (middle right panel). These differences with the classical case can be understood by plotting cuts of the Wigner distribution at constant energy $\hbar\omega = \pm 11 \mu\text{eV}$ (lower panels of Fig. 3). In the classical case the sizeable values of the high harmonics of the Wigner distribution are necessary to reconstruct an equilibrium Fermi distribution which varies sharply from 0 to 1. On the contrary, high harmonics are suppressed in the quantum case such that $W_S^{(e)}(t, \omega)$ varies in

a much smoother way. This explains the overshoots (undershoots) above 1 (below 0) which agree well with theoretical expectations (plain lines).

The second step of our quantum signal dissection scheme extracts individual electronic wavepackets from the reconstructed Wigner distribution. This reconstruction is performed on the excess single electron coherence^{28,29} $\Delta_0 \mathcal{G}_S^{(e)}(t + \frac{\tau}{2}, t - \frac{\tau}{2})$, which is the inverse Fourier transform with respect to ω of the excess Wigner distribution $\Delta_0 W_S^{(e)}(t, \omega) = W^{(e)}(t, \omega) - \Theta(-\omega)$, defined with respect to the zero temperature Fermi electronic distribution function $\Theta(-\omega)$. This reference choice ensures that all excitations, including the thermal ones, are extracted by our algorithm. The goal is to find the simplest expression of the excess single electron coherence in terms of recently introduced "electronic atoms of signal"⁴, which form a

$$\Delta_0 \mathcal{G}_S^{(e)}(t, t') = \sum_{(l, l') \in \mathbb{Z}^2} \left[g^{(e)}(l - l') \varphi_l^{(e)}(t) \varphi_{l'}^{(e)}(t')^* - g^{(h)}(l - l') \varphi_l^{(h)}(t) \varphi_{l'}^{(h)}(t')^* + 2\Re \left(g^{(eh)}(l - l') \varphi_l^{(e)}(t) \varphi_{l'}^{(h)}(t')^* \right) \right] \quad (4)$$

When $l = l'$, the real numbers $0 \leq g^{(e)}(0) \leq 1$ and $0 \leq g^{(h)}(0) \leq 1$ represent the probability for emitting an electronic (resp. hole) excitation with wavefunction $\varphi^{(e)}$ (resp. $\varphi^{(h)}$) at each period. When $l \neq l'$, the complex numbers $g^{(e)}(l - l')$ (resp. $g^{(h)}(l - l')$) represent the interperiod coherence between electronic (resp. hole) wavepackets. Finally, the complex number $g^{(eh)}(l - l')$ represents the electron/hole coherence between the electron and hole wavepacket associated with periods l and l' . These terms occur when the probability to emit the electron and hole excitations differ from 1, such that a coherent superposition between the equilibrium state and the creation of an electron/hole pair is generated. They encode the modulus and phase of this coherent superposition. By exact diagonalization of the projection of the excess single electron coherence on the electronic and hole sectors (see Supplementary Material) it is possible to extract from $W_S^{(e)}$ the electron and hole wavefunctions $\varphi^{(e/h)}$ as well as the interperiod coherences $g^{(e)}(l - l')$, $g^{(h)}(l - l')$ and $g^{(eh)}(l - l')$. These data describe the single particle content of the electronic current and quantify how far it deviates from the ideal electron and hole emission regime, characterized in this language by $g^{(eh)}(l - l') = 0$ and $g^{(e)}(l - l') = g^{(h)}(l - l') = \delta_{l, l'}$.

Figure 4 presents the result of this analysis on the experimental data obtained for the quantum drive ($f = 9$ GHz). As expected, the excess coherence is strongly dominated by one electronic $\varphi^{(e)}$ and one hole $\varphi^{(h)}$ wavepacket, which are plotted in the Wigner representation on the upper and middle panels. The hole is shifted by half a period with respect to the electron and its energy dependence is almost the same as that of the electron's at positive energy, as can be seen from their electronic distribution functions $f|\varphi^{(e/h)}(\omega)|^2$. Note that these functions present almost flat plateaus of width hf : devi-

family of normed and mutually orthogonal electronic wavelets representing the electron and hole wavefunctions generated for each time period of the source. Generically, several electron/hole wavelets are needed, since several electron/hole excitations might be emitted in different wavepackets for each period of the source. However, in our experimental situation at $f = 9$ GHz, and more generally whenever the probability to emit more than one electron/hole pair per period is very small, only one electron $\varphi^{(e)}$ and one hole $\varphi^{(h)}$ wavelets are needed. The time translated wavepackets $\varphi_l^{(\alpha)}(t) = \varphi^{(\alpha)}(t - lT)$ are defined using the period index $l \in \mathbb{Z}$ and satisfy the following orthogonality conditions $\langle \varphi_l^{(\alpha)} | \varphi_{l'}^{(\beta)} \rangle = \delta_{\alpha, \beta} \delta_{l, l'}$ for α and β being e or h . The simplest generic form of the excess single electron coherence can then be written in this case as:

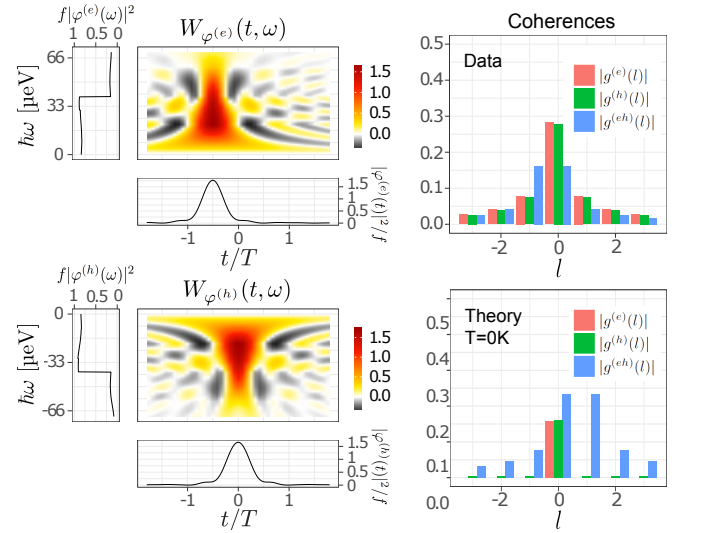


FIG. 4. Left panel: Wigner distribution functions $W_{\varphi^{(e/h)}}(t, \omega) = \int d\tau \varphi^{(e/h)}(t + \frac{\tau}{2}) \varphi^{(e/h)*}(t - \frac{\tau}{2}) e^{i\omega\tau}$ for the dominant electronic $\varphi^{(e)}$ and hole $\varphi^{(h)}$ atoms of signal in the $f = 9$ GHz case. The panels in the margins of the colour plots represent the time $|\varphi^{(e/h)}(t)|^2/f$ and energy $f|\varphi^{(e/h)}(\omega)|^2$ distributions obtained by integration of $W_{\varphi^{(e/h)}}(t, \omega)$ over ω and t . Right panel: moduli of the interperiod coherence $|g^{(e)}(l)|$, $|g^{(h)}(l)|$ and $|g^{(eh)}(l)|$ (Data and numerical simulation at $T_{el} = 0$ mK)

ations from flatness express that atoms of signal at finite temperature are contaminated by thermal excitations. The moduli of the corresponding interperiod coherences are depicted on the right panel: they extend beyond one period, as expected, since the thermal coherence time $\hbar/k_B T_{el} \simeq 0.5$ ns is roughly

4 times larger than the period. Since $g^{(eh)}(l - l') \neq 0$ and both $g^{(e)}(0) \simeq g^{(h)}(0) \simeq 0.27 \neq 1$, we are not in the single electron regime. The specific role of thermal fluctuations is illustrated by comparing on Figure 4 the data ($T_{\text{el}} = 100$ mK) with the numerical simulation of the interperiod coherences in the zero temperature case. The occupation probabilities $g^{(e)}(0)$ and $g^{(h)}(0)$ increase from 0.16 ($T_{\text{el}} = 0$ mK) to 0.27 ($T_{\text{el}} = 100$ mK) when the temperature increases, reflecting the contamination by thermal excitations populating $\varphi^{(e/h)}$. Thermal fluctuations also decrease the electron/hole coherence $|g^{(eh)}(0)|$, showing how temperature progressively destroys the coherent superposition between the equilibrium state and the creation of an electron/hole pair.

To conclude, we have demonstrated a quantum electrical current analyzer which directly extracts the single electron and hole wavefunctions, as well as their emission probabilities and coherence from one emission period to the other. Assuming a minimal knowledge on the state of the electron fluid, it can be used to characterize any quantum electrical current. It also explicitly takes into account the role

of thermal excitations and their progressive contamination of the electron and hole wavefunctions. The same principle could lead to quantum current analyzers for any low-dimensional conductor that can be weakly tunnel-coupled to a probe port for noise measurements, enabling the control of the quantum state of the elementary excitations transferred across nanoscale conductors. Our quantum analyzer is the tool of choice for single electron source characterization or for identifying single particle wavefunctions generated in interacting conductors³¹. It may also offer a way to access to the recently studied electron/hole entanglement³² and, supplemented by other measurements³³, to quantify more precisely the importance of interaction-induced quantum correlations. Finally, it can establish a bridge between electron and microwave quantum optics^{34,35}, by probing the electronic content of microwave photons injected from a transmission line into a quantum conductor.

This work has been supported by ANR grants “1shot reloaded” (ANR-14-CE32-0017), and ERC consolidator grant “EQuO” (No. 648236).

-
- ¹ Gwendal Fève, Adrien Mahé, Jean-Marc Berroir, Takis Kontos, Bernard Plaças, Christian Glatli, A. Cavanna, Bernard Etienne, and Yong Jin, An On-Demand Coherent Single Electron Source, *Science* **316**, 1169 (2007).
- ² C. Leicht, P. Mirovsky, B. Kaestner, F. Hohls, V. Kashcheyevs, E.V. Kurganova, U. Zeitler, T. Weimann, K. Pierz, and H.W. Schumacher, Generation of energy selective excitations in quantum Hall edge states, *Semiconductor Science and Technology* **26**, 055010 (2011).
- ³ J Dubois, T Jullien, F Portier, P Roche, A Cavanna, Y Jin, W Wegscheider, P Roulleau, and D C Glatli, Minimal-excitation states for electron quantum optics using levitons, *Nature*, **502**, 659 (2013).
- ⁴ J. D. Fletcher, P. See, H. Howe, M. Pepper, S. P. Giblin, J. P. Griffiths, G. A. C. Jones, I. Farrer, D. A. Ritchie, T. J. B. M. Janssen, and M. Kataoka, Clock-controlled emission of single-electron wave packets in a solid-state circuit, *Phys. Rev. Lett.* **111**, 216807 (2013).
- ⁵ M. Büttiker, Y. Imry, and R. Landauer, and S. Pinhas, Generalized many-channel conductance formula with application to small rings, *Phys. Rev. B* **31**, 6207 (1985).
- ⁶ M. Kataoka, N. Johnson, C. Emary, P. See, J. P. Griffiths, G. A. C. Jones, I. Farrer, D. A. Ritchie, M. Pepper, and T. J. B. M. Janssen, Time-of-flight measurements of single-electron wave packets in quantum hall edge states, *Phys. Rev. Lett.* **116**, 126803 (2016).
- ⁷ C. Altimiras, H. le Sueur, U. Gennser, A. Cavanna, D. Mailly, and F. Pierre, Non-equilibrium edge-channel spectroscopy in the integer quantum Hall regime, *Nature Physics* **6**, 34 (2009).
- ⁸ Mihajlo Vanević, Yuli V. Nazarov, and Wolfgang Belzig, Elementary events of electron transfer in a voltage-driven quantum point contact, *Phys. Rev. Lett.* **99**, 076601 (2007).
- ⁹ Mihajlo Vanević, Julien Gabelli, Wolfgang Belzig, and Bertrand Reulet, Electron and electron-hole quasiparticle states in a driven quantum contact, *Phys. Rev. B* **93**, 041416 (2016).
- ¹⁰ T. Jullien, P. Roulleau, B. Roche, a. Cavanna, Y. Jin, and D. C. Glatli, Quantum tomography of an electron, *Nature* **514**, 603 (2014).
- ¹¹ Lee H. Levitov, L. S. and G. Lesovik. Electron counting statistics and coherent states of electric current. *J. Math. Phys.* **37**, 4845 (1996).
- ¹² Klich I. Keeling, J. and L. Levitov, Minimal excitation states of electrons in one dimensional wires, *Phys. Rev. Lett.* **97** 116403, (2006).
- ¹³ R. C. Liu, B. Odom, Y. Yamamoto, and S. Tarucha, Quantum interference in electron collision, *Nature* **391**, 263 (1998).
- ¹⁴ I. Neder, N Ofek, Y. Chung, M. Heiblum, D. Mahalu, and V. Umansky, Interference between two indistinguishable electrons from independent sources, *Nature* **448**, 333 (2007).
- ¹⁵ S. Ol'khovskaya, J. Splettstoesser, M. Moskalets, and M. Büttiker, Shot noise of a mesoscopic two-particle collider, *Phys. Rev. Lett.* **101**, 166802 (2008).
- ¹⁶ E Bocquillon, V Freulon, P Degiovanni, B Plaças, A Cavanna, and Y Jin, Coherence and indistinguishability of single electron wavepackets emitted by independent sources, *Science* **339**, 1054 (2013).
- ¹⁷ D. Ferraro, A. Feller, A. Ghibaudo, E. Thibierge, E. Bocquillon, G. Fève, Ch. Grenier, and P. Degiovanni, Wigner function approach to single electron coherence in quantum Hall edge channels, *Phys. Rev. B* **88** 205303 (2013).
- ¹⁸ Vyacheslavs Kashcheyevs and Peter Samuelsson, Classical-to-quantum crossover in electron on-demand emission, *Phys. Rev. B* **95**, 245424 (2017).
- ¹⁹ P. Bertet, A. Auffeves, P. Maioli, S. Osnaghi, T. Meunier, M. Brune, J. M. Raimond, and S. Haroche, Direct Measurement of the Wigner Function of a One-Photon Fock State in a Cavity, *Phys. Rev. Lett.* **89**, 200402 (2002).
- ²⁰ D. Leibfried, D. M. Meekhof, B. E. King, C. Monroe, W. M. Itano, and D. J. Wineland, Experimental Determination of the Motional Quantum State of a Trapped Atom, *Phys. Rev. Lett.* **77**, 4281 (1996).
- ²¹ T. J. Dunn, I. A. Walmsley, and S. Mukamel, Experimental Determination of the Quantum-Mechanical State of a Molecular Vibrational Mode Using Fluorescence Tomography, *Phys. Rev. Lett.* **74**, 884 (1995).
- ²² Ch Grenier, R Hervé, E Bocquillon, F D Parmentier, B Plaças, J M Berroir, G Fève, and P Degiovanni, Single-electron quan-

- tum tomography in quantum Hall edge channels, *New Journal of Physics* **13**, 093007 (2011).
- ²³ Ou Z. Y. Hong, C. K. and L. Mandel, Measurement of subpicosecond time intervals between two photons by interference, *Phys. Rev. Lett.* **59**, 2044 (1987).
- ²⁴ Julien Gabelli and Bertrand Reulet, Shaping a time-dependent excitation to minimize the shot noise in a tunnel junction, *Phys. Rev. B* **87**, 075403 (2013).
- ²⁵ N. Wiener, *Extrapolation, Interpolation, and Smoothing of Stationary Time Series*, Wiley and Sons, 1949.
- ²⁶ L.-H. Reydellet, P. Roche, D. C. Glatli, B. Etienne, and Y. Jin, Quantum partition noise of photon-created electron-hole pairs, *Phys. Rev. Lett.* **90**, 176803 (2003).
- ²⁷ Valentin S. Rychkov, Mikhail L. Polianski, and Markus Büttiker, Photon-assisted electron-hole shot noise in multiterminal conductors, *Phys. Rev. B* **72**, 155326 (2005).
- ²⁸ E. Bocquillon, V. Freulon, F.D. Parmentier, J.-M. Berroir, B. Plaçais, C. Wahl, J. Rech, T. Jonckheere, T. Martin, C. Grenier, D. Ferraro, P. Degiovanni, and G. Fève, Electron quantum optics in ballistic chiral conductors, *Ann. Phys.* **526**, 1 (2014).
- ²⁹ G. Haack, M. Moskalets, and M. Büttiker, Glauber coherence of single-electron sources, *Phys. Rev. B*, **87**, 201302 (2013).
- ³⁰ B. Roussel, C. Cabart, G. Fève, E. Thibierge, and P. Degiovanni, Electron quantum optics as quantum signal processing, *Physica Status Solidi B* **254**, 16000621 (2017).
- ³¹ A. Marguerite, C. Cabart, C. Wahl, B. Roussel, V. Freulon, D. Ferraro, Ch. Grenier, J.-M. Berroir, B. Plaçais, T. Jonckheere, J. Rech, T. Martin, P. Degiovanni, A. Cavanna, Y. Jin, and G. Fève, Decoherence and relaxation of a single electron in a one-dimensional conductor, *Phys. Rev. B* **94** 115311 (2016).
- ³² P.P. Hofer, D. Dasenbrook, and C. Flindt, On-demand entanglement generation using dynamic single electron sources, *Physica Status Solidi B* **254**, 1600582 (2017).
- ³³ É. Thibierge, D. Ferraro, B. Roussel, C. Cabart, A. Marguerite, G. Fève, and P. Degiovanni, Two-electron coherence and its measurement in electron quantum optics, *Phys. Rev. B* **93**, 081302 (2016).
- ³⁴ A.L. Grimsmo, F. Qassemi, , B. Reulet, and A. Blais, Quantum optics theory of electronic noise in quantum conductors, *Phys. Rev. Lett.* **116**, 043602 (2015).
- ³⁵ Stéphane Virally, Jean Olivier Simoneau, Christian Lupien, and Bertrand Reulet, Discrete photon statistics from continuous microwave measurements, *Phys. Rev. A* **93**, 043813 (2016).

Appendix A: Sample and noise measurements

The sample is a GaAs/AlGaAs two dimensional electron gas of nominal density $n_s = 1.9 \times 10^{15} \text{ m}^{-2}$ and mobility $\mu = 2.4 \times 10^6 \text{ cm}^{-2} \text{ V}^{-1} \text{ s}^{-1}$. It is placed in a magnetic field $B = 3.7 \text{ T}$ to reach the quantum Hall regime at filling factor $\nu \approx 2$ in the bulk. The current noise at the output of the quantum point contact is converted to a voltage noise on the resistance $R = h/2e^2$ (at filling factor $\nu = 2$) between the ohmic contact connected to output 3 of the splitter and an ohmic contact connected to the ground. The contact on output 3 is connected to a tank circuit so as to move the noise measurement frequency to 1.45 MHz with a 78 kHz bandwidth. The tank circuit is followed by a pair of homemade cryogenic amplifiers followed by room temperature amplifiers and a vector signal analyzer in order to measure the voltage correlations between the two amplification chains. Noise measurements are calibrated by measuring both the thermal noise of the output resistance R , and the partition noise of a d.c. bias applied on input 2 of the electronic beam-splitter.

Appendix B: Reconstruction of $\Delta W_{S,n}^{(e)}(\omega)$ from noise measurements

The excess electronic distribution function $\Delta W_{S,n=0}^{(e)}(\omega)$ can be obtained via the derivative of ΔS with respect to the d.c. bias ω_{DC} applied on the probe port.

$$\Delta S = 2e^2 \mathcal{T}(1 - \mathcal{T}) \int \frac{d\omega}{2\pi} \left[\overline{\Delta W_S^{(e)}}^t (1 - 2f_{\text{eq}}) - 2 \overline{\Delta W_S^{(e)} \Delta W_{P_n}^{(e)}}^t \right] \quad (\text{B1})$$

$$\widetilde{\Delta W}_{S,0}^{(e)} = -\frac{\pi}{2e^2 \mathcal{T}(1 - \mathcal{T})} \frac{\partial \Delta S}{\partial \omega_{\text{DC}}} = \int d\omega \Delta W_{S,0}^{(e)}(\omega) \left(\frac{-\partial f_{\text{eq}}}{\partial \omega} \right) (\omega - \omega_{\text{DC}}) \quad (\text{B2})$$

As shown by Eq.(B2), the experimental signal $\widetilde{\Delta W}_{S,0}^{(e)}$ does not provide directly $\Delta W_{S,0}^{(e)}$ but its convolution with the thermally broadened function $\left(\frac{-\partial f_{\text{eq}}}{\partial \omega} \right)$. Knowing the electronic temperature and using deconvolution techniques based on Wiener filtering¹ (see next section), one can reconstruct $\Delta W_{S,0}^{(e)}(\omega)$ from the measurement of $\widetilde{\Delta W}_{S,0}^{(e)}$.

The higher order terms $\Delta W_{S,n \neq 0}^{(e)}$ which encode all the time dependence, are reconstructed from the measurement of the output noise ΔS_ϕ as a function of the phase ϕ of a.c. voltage $V_{P_n}(t)$ and of the d.c. voltage ω_{DC} applied on the probe port. Using Eqs.(B1) with $\Delta W_{P_n}^{(e)}(t, \omega) = -\frac{eV_{P_n}}{\hbar} \cos(2\pi nft + \phi)g_n(\omega - \omega_{\text{DC}})$, we can reconstruct the real and imaginary parts of $\Delta W_{S,n}^{(e)}$:

$$\Re(\widetilde{\Delta W}_{S,n}^{(e)}) = \frac{h}{8e^3 V_{P_n} \mathcal{T}(1 - \mathcal{T})} (\Delta S_{\phi=0} - \Delta S_{\phi=\pi}) = \int d\omega \Re(\Delta W_{S,n}^{(e)}(\omega)) g_n(\omega - \omega_{\text{DC}}) \quad (\text{B3a})$$

$$\Im(\widetilde{\Delta W}_{S,n}^{(e)}) = \frac{h}{8e^3 V_{P_n} \mathcal{T}(1 - \mathcal{T})} (\Delta S_{\phi=\frac{\pi}{2}} - \Delta S_{\phi=\frac{3\pi}{2}}) = \int d\omega \Im(\Delta W_{S,n}^{(e)}(\omega)) g_n(\omega - \omega_{\text{DC}}) \quad (\text{B3b})$$

As in the $n = 0$ case, the experimental signal is the convolution between $\Delta W_{S,n}^{(e)}$ and $g_n = \left(f_{\text{eq}}(\omega - n\pi f) - f_{\text{eq}}(\omega + n\pi f) \right) / (2\pi n f)$. The real and imaginary parts of $\Delta W_{S,n}^{(e)}$ are thus reconstructed using the Wiener filtering deconvolution technique (see next section). A specific difficulty arises for the $n \neq 0$ terms, as their reconstruction process requires the accurate knowledge of the relative phases between the probe signals for various values of n . To measure the phase relationship between the $n = 1$, $n = 2$ and $n = 3$ probe signals, we use two-particle interferences between two different probe signals generated simultaneously at input 2 in the absence of the source (e.g. between $n = 1$ and $n = 2$ or between $n = 1$ and $n = 3$). The noise at the splitter output is then minimal when the two probe signals are in phase, allowing for an accurate calibration of the relative phase between the probe signals for different harmonics n . For the measurement of the phase between the $n = 2$ and $n = 1$ harmonics, two-particle interferences between source and probe vanish at zero bias voltage V_{DC} due to the electron/hole symmetry of a sinusoidal drive. We thus add a small positive bias voltage to the probe port in order to calibrate the relative phase (this method should be applied for the phase calibration of all even harmonics). As a result of the phase calibration, we find that, as theoretically expected for sine drives, $\Im(\widetilde{\Delta W}_{S,n}^{(e)}) = 0$ for all n and all ω . The reconstruction of $\Delta W_{S,n \neq 0}^{(e)}$ also requires the accurate knowledge of the probe voltage amplitude V_{P_n} which are calibrated by measuring the partition noise of the probe (source switched off) as a function of the drive amplitude V_{P_n} . When measuring these $n \neq 0$ harmonics, we also systematically checked the linear dependence of the output noise with the probe amplitude in order to check the validity of the linear approximation relating $\Delta W_{P_n}^{(e)}(t, \omega)$ to $V_{P_n}(t)$.

Appendix C: Wiener deconvolution filter

In order to account for the convolution of $\Delta W_{S,n}^{(e)}$ with g_n , the noise data $\widetilde{\Delta W}_{S,n}^{(e)}$ is deconvoluted using a Wiener deconvolution filter¹. Given our experimental situation, where g_n is well known, but the experimental data $\widetilde{\Delta W}_{S,n}^{(e)}$ is spoiled by noise, brute force deconvolution techniques cannot be applied as they tend to amplify the noise fluctuations. On the contrary, the Wiener filter allows to efficiently deconvolute the signal while smoothing the random fluctuations. Denoting by FT and FT^{-1} the Fourier and inverse Fourier transformations, which relate the variable ω to its conjugate variable $\tilde{\omega}$, we define the signal over noise ratio of the measurement: $\rho(\tilde{\omega}) = \frac{|FT[g_n] \cdot FT[\Delta W_{S,n}^{(e)}]|^2(\tilde{\omega})}{N(\tilde{\omega})}$, where $N(\tilde{\omega})$ is the power spectral density of the experimental noise. The Wiener filter that deconvolutes the noisy experimental data is then defined as:

$$\Delta W_{S,n}^{(e)}(\omega) = FT^{-1} \left[H^*(\tilde{\omega}) \cdot FT \left[\widetilde{\Delta W}_{S,n}^{(e)} \right] (\tilde{\omega}) \right] \quad (C1)$$

$$H(\tilde{\omega}) = \frac{1}{FT[g_n](\tilde{\omega})} \frac{1}{1 + \rho^{-1}(\tilde{\omega})} \quad (C2)$$

For $\tilde{\omega}$ values such that the signal to noise ratio is high ($\rho^{-1}(\tilde{\omega}) \ll 1$), the Wiener filter acts as a standard deconvolution filter: $H = 1/FT[g_n]$. On the contrary, $\tilde{\omega}$ values which do not carry information on the signal ($\rho^{-1}(\tilde{\omega}) \gg 1$) are suppressed by the Wiener filter: $H \approx 0$, so that contrary to standard deconvolution methods, the noise does not get amplified by the deconvolution but is instead suppressed in the process. The difficulty is then to properly evaluate $\rho(\tilde{\omega})$. Assuming no correlations between the fluctuations of $\Delta W_{S,n}^{(e)}$ measured at different energies ω (set by the d.c. bias ω_{DC}), meaning that $N(\tilde{\omega}) = N$ is a white noise, the value of N is directly set by the size of the experimental error bars on the measurement of ΔS . If the noise $N(\tilde{\omega})$ is known, it is not the case for the signal $FT[\Delta W_{S,n}^{(e)}](\tilde{\omega})$ which is the quantity to be determined. We have tested two different methods for estimating ρ , which give equivalent results within error bars. The first method relies on an estimate of the signal over noise ratio using a theoretical prediction for $FT[\Delta W_{S,n}^{(e)}](\tilde{\omega})$. In the second method $\rho(\tilde{\omega})$ is self-consistently determined from an optimization of the deconvolution process. More precisely, we take $\rho(\tilde{\omega}) = \left| FT[g_n] \cdot FT[\widetilde{\Delta W}_{S,n}^{(e)}] \right|^2(\tilde{\omega})/a$, where a is self-consistently determined. The optimization is based on the balance between two limits. When ρ is overestimated (meaning that the chosen a is too small), the deconvolution amplifies $\tilde{\omega}$ values which are in fact dominated by the noise which results in the appearance of high frequency fluctuations in the deconvoluted signal. When ρ is underestimated (meaning that the chosen a is too large), $\tilde{\omega}$ values which are dominated by the signal are suppressed by the Wiener filter and the resulting deconvoluted data is oversmoothed. It can be detected by reapplying the convolution by g_n on the deconvoluted signal; oversmoothing then shows up as a result which differs from the experimentally measured data $\widetilde{\Delta W}_{S,n}^{(e)}$. This method leads to an uncertainty in the determination of ρ (related to the uncertainty on the parameter a) which, together with the noise on the experimental data, are taken into account when evaluating the error bar of the deconvoluted data. In order to evaluate these error bars, we generate a random distribution of experimental data (with a standard deviation given by the experimental uncertainty) and a family of Wiener deconvolution filters with randomly distributed values of ρ (with a standard deviation given by the uncertainty on the determination of ρ). We deconvolute the randomly picked data with a randomly chosen filter, generating a random distribution of deconvoluted data. The data points of $\Delta W_{S,n}^{(e)}$ plotted on Fig.(2) and Fig.(3) correspond to the average of the obtained distribution and the error bars to its standard deviation.

Appendix D: Electron and hole wavefunction extraction

The extraction of electron and hole wavefunctions from the experimental data of $\Delta W_S^{(e)}(t, \omega)$ relies on an algorithm which recasts any excess T -periodic single electron coherence $\Delta_0 \mathcal{G}^{(e)}$ under the form given by Eq.(4) of the article:

$$\begin{aligned} \Delta_0 \mathcal{G}_S^{(e)}(t, t') = & \sum_{(l, l') \in \mathbb{Z}^2} \left(g^{(e)}(l - l') \varphi_l^{(e)}(t) \varphi_{l'}^{(e)}(t')^* - g^{(h)}(l - l') \varphi_l^{(h)}(t) \varphi_{l'}^{(h)}(t')^* \right) \\ & + \sum_{(l, l') \in \mathbb{Z}^2} \left(g^{(eh)}(l - l') \varphi_l^{(e)}(t) \varphi_{l'}^{(h)}(t')^* + \text{h.c.} \right) \end{aligned} \quad (D1)$$

The algorithm is based on an exact diagonalization of the projection of $\Delta_0 \mathcal{G}_S^{(e)}$ onto the electronic and hole quadrants containing the information on the purely electronic and purely hole single particle excitations within the system. Due to time periodicity, this leads to electronic and hole probability spectra consisting of bands on the quasi-pulsation interval $0 \leq \nu \leq 2\pi f$ associated with the time period T as well as eigenvectors which are the Floquet version of Bloch waves of solid state physics². The analogous of Wannier functions³ are then the electronic and hole atoms of signal⁴. As in solid state physics⁵, the ambiguity of these wavepackets has been lifted by minimizing their time spreading. Finally, the electron and hole coherences $g^{(e)/h}(l)$ ($l \in \mathbb{Z}$) can be obtained from the probability spectras and the electron/hole coherences computed from $\Delta_0 \mathcal{G}^{(e)}$ using the explicit numerical data for the electronic and hole atoms of signals².

After Wiener filtering, the experimental data come as a finite set of real values $\Delta W_{S,n}^{(e)}(\omega_k)$ where ω_k are the discretized values of ω and $n = 0, \pm 1, \pm 2$. First we add the thermal excess $f_{eq}(\omega) - \Theta(-\omega)$ of the equilibrium Fermi Dirac

distribution at temperature $T_{el} = 100$ mK to $\Delta W_{S,n=0}^{(e)}(\omega)$ to obtain the experimental dataset for $\Delta_0 W_S^{(e)}(\omega)$. Then, in order to extract a square matrix for the exact diagonalization, the first step is to generate new data that can be matched on a grid well suited to the electronic and hole quadrants. These two quadrants are defined in the frequency domain as corresponding to the sectors where purely electronic (resp. purely hole) excitation contribute to $\Delta W_{S,n}^{(e)}(\omega)$. For a periodically driven source, these sectors correspond to $\omega \pm n\pi f \geq 0$ for the electron quadrant and to $\omega \pm n\pi f \leq 0$ for the hole quadrant⁶. For each n , the dataset $\Delta_0 W_{S,n}^{(e)}(\omega_k)$ is first interpolated using cubic splines to infer a new dataset on a grid adapted to the electronic and hole quadrants, that is such that this grid intersects the boundaries $\omega \pm n\pi f = 0$ of the electronic and hole quadrants. This new data grid has a discretization step $\delta\omega$ such that $\hbar\delta\omega \simeq 0.19 \mu\text{eV}$. We assign zero to the remaining grid points for which no data is available (higher harmonics $|n| > 2$ and values of $\hbar|\omega| \gtrsim 70 \mu\text{eV}$). This dataset is then used to build the matrices corresponding to the projection of this interpolated data for $\Delta W_{S,n}^{(e)}(\omega)$, which are then fed into the electron and hole wavefunction algorithm.

¹ N. Wiener, *Extrapolation, Interpolation, and Smoothing of Stationary Time Series*, Wiley and Sons, 1949.

² B. Roussel and P. Degiovanni, In preparation, 2017.

³ G.H. Wannier, The structure of electronic excitation levels in insulating crystal, *Physical Review* **52**, 191 (1937).

⁴ B. Roussel, C. Cabart, G. Fève, E. Thibierge, and P. Degiovanni, Electron quantum optics as quantum signal processing, *Physica Status Solidi B* **254**, 16000621 (2017).

⁵ N. Marzari, A. A. Mostofi, R. J. Yates, I. Souza, Ivo and D. Vanderbilt, Maximally localized Wannier functions: Theory and applications, *Rev. Mod. Phys.* **84**, 1419 (2012).

⁶ D. Ferraro, A. Feller, A. Ghibaudo, E. Thibierge, E. Bocquillon, G. Fève, Ch. Grenier, and P. Degiovanni, Wigner function approach to single electron coherence in quantum Hall edge channels, *Phys. Rev. B* **88** 205303 (2013).